



HAL
open science

Cathodoluminescence and microstructural analysis of amorphous yttrium-aluminum-borate luminescent powders

Atul D. Sontakke, Lisa I.D.J. Martin, Victor Castaing, Bruno Viana, Philippe
Smet

► **To cite this version:**

Atul D. Sontakke, Lisa I.D.J. Martin, Victor Castaing, Bruno Viana, Philippe Smet. Cathodoluminescence and microstructural analysis of amorphous yttrium-aluminum-borate luminescent powders. *Journal of Luminescence*, 2019, 215, pp.116669. 10.1016/j.jlumin.2019.116669 . hal-02303375

HAL Id: hal-02303375

<https://hal.science/hal-02303375>

Submitted on 20 Dec 2021

HAL is a multi-disciplinary open access archive for the deposit and dissemination of scientific research documents, whether they are published or not. The documents may come from teaching and research institutions in France or abroad, or from public or private research centers.

L'archive ouverte pluridisciplinaire **HAL**, est destinée au dépôt et à la diffusion de documents scientifiques de niveau recherche, publiés ou non, émanant des établissements d'enseignement et de recherche français ou étrangers, des laboratoires publics ou privés.



Distributed under a Creative Commons Attribution - NonCommercial 4.0 International License

Cathodoluminescence and microstructural analysis of amorphous Yttrium-Aluminum-Borate luminescent powders

Atul D. Sontakke,^{a,b,c} Lisa I. D. J. Martin,^a Victor Castaing,^b Bruno Viana,^b Philippe F. Smet^a

^a*LumiLab, Department of Solid State Sciences, Ghent University, 9000 Ghent, Belgium*

^b*PSL Research University, Chimie ParisTech – CNRS, Institut de Recherche de Chimie Paris, 75005 Paris, France*

^c*Condensed Matter and Interfaces, Debye Institute for Nanomaterials Science, Utrecht University, Princetonplein 1, 3584 CC Utrecht, The Netherlands*

Abstract

We present the cathodoluminescence (CL) and microstructural analysis of amorphous yttrium aluminum/aluminium borate (a-YAB) luminescent powders synthesized by polymeric precursor (PP) and sol-gel (SG) based wet-chemical methods. The a-YAB powders exhibit bright photoluminescence tunable from intense blue to white chromaticity region depending on their calcination temperature. Here, the influence of calcination temperature on CL and microstructural properties of the a-YAB powders has been investigated. The a-YAB powders showed weak but homogeneous CL. Within the optimum calcination temperatures for photoluminescence (650-740°C for PP and 450-600°C for SG series), the CL observed to be more intense for powders synthesized at higher calcination temperature. The microstructure analysis revealed that the SG series powders calcined below 570°C exhibit intraparticle chemical inhomogeneity, whereas no such inhomogeneity could be seen in PP series powders, owing to their higher calcination temperatures. Nevertheless, both series exhibit similar luminescence broadening with calcination temperatures despite these microscopic differences, revealing that the luminescence broadening does not depend on the chemical properties at the microscopic level, but is controlled by more intrinsic effects on the luminescent centers or its immediate surrounding as a function of calcination temperature.

Introduction

The wet-chemically synthesized amorphous yttrium aluminum borate (a-YAB) powders, with a chemical composition close to that of crystalline $\text{YAl}_3(\text{BO}_3)_4$, exhibit bright photoluminescence (PL) [1]. The origin of this luminescence has recently been ascribed to the presence of organic molecules trapped inside the inorganic glassy matrix during the synthesis process and their subsequent evolution with thermal treatment [1,2]. The powders exhibit intense blue to broadband white emission depending on their thermal history as well as their synthesis methods (Figure 1). We have recently reported the polymeric precursor (PP) and sol-gel (SG) based wet-chemical methods to synthesize micrometer sized amorphous a-YAB powders [1-3]. In PP method syntheses, relatively high calcination temperatures (650-740°C) are necessary to achieve optimum luminescence over the SG method syntheses (450-600°C). Nevertheless, in both series a similar luminescence broadening is witnessed within the investigated temperature ranges.

To further develop this type of luminescence in the framework of luminescent probes [4,5] or light emitting devices [6], it is imperative to have a good understanding on the origin of the luminescence centers and its broadening phenomenon. While the broad emission spectrum is advantageous for the use of these phosphors in solid state lighting devices with high color rendering, the rather strong emission in the violet to blue part of the visible spectrum limits the overall luminous efficacy [7]. It is therefore vital to be able to control and optimize the luminescence properties. In contrast to luminescence based on lanthanides (e.g. Eu^{2+} , Ce^{3+} or the 4f-4f emitting ions) [8-10] or transition metals (e.g. Cr^{3+} or Mn^{4+}) [11,12], where the emission spectrum can roughly be predicted based on the type of transition and the local environment of the dopant, this structural-luminescence relationship has not yet fully been established in the a-YAB powders, which lack a traditional dopant ion.

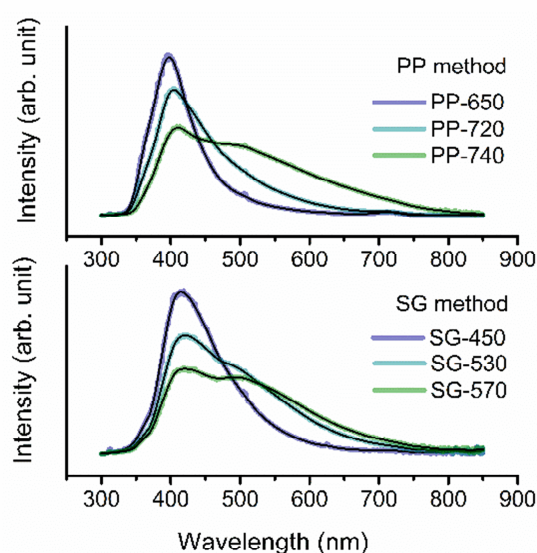


Figure 1: PL spectra of a-YAB powders obtained by sol-gel (SG) and polymeric precursor (PP) methods. The PL were recorded under 254 nm excitation to achieve complete spectral profiles. The powders are denoted by SG-x and PP-x, where x represents the calcination temperature in °C for both studied synthesis routes.

Moreover, due to the inorganic refractory-type nature of the a-YAB host material, it is difficult to extract the trapped organic species in intact form for chemical analysis [13,14]. The complementary solid-state analytical techniques (including NMR, EPR, ENDOR, etc.) revealed the presence of small polyaromatic hydrocarbons (PAH), which exhibit good correlation with the broadening of the luminescence spectral profiles [2]. A parallel approach using time-gated spectroscopy and energy level modeling hinted to the presence of multiple emitting centers, which undergo a systematic evolution in relative strengths as a function of calcination temperature, thereby causing the spectral broadening [15]. Each emitting center exhibits fluorescence as well as phosphorescence components, and therefore the complete spectrum becomes an admixture of several emission bands. Based on the time-gated spectroscopy and theoretical modelling using DFT calculations, we could construct the energy level structure of first few prominent emitting centers and identify the higher energy violet-blue region emitting center to be a phenalene based compound [15]. The results also indicated that the primary energy level structure of the other luminescent centers might be similar but with decreasing energy gaps that lead to the red shifted emissions. This suggested that the broadening might be associated with the bathochromic effect in luminophore compounds. The bathochromic spectral shift can arise due to a π -conjugation in organic molecules, a change in the functional group, or a variation in chemical environment [16]. During the calcination step in wet-chemical synthesis methods, the primary network structure undergoes densification. Simultaneously, the solid-gas reactions take place inside the powder grains through diffusion, leading to complex molecular reactions. These interactions during calcination process can modify the luminescent compounds as well as chemical properties of the host, responsible for the luminescence properties of the a-YAB powders.

In the present study, the microstructural properties of a-YAB powders as a function of calcination temperatures have been investigated using scanning electron microscopy and cathodoluminescence (CL) in order to seek a correlation between the microstructure and the luminescence properties. CL spectroscopy is a vital technique to unravel the hidden details of functional luminescent materials at microscopic levels, which collectively represents their bulk performances [17-22]. A scanning electron microscope (SEM) was used to study the microstructure evolution, while simultaneously recorded energy dispersive X-ray (EDX) elemental mapping and CL microscopy provided further insights on the structure-property relationship.

Experimental details

Two series of a-YAB powders obtained by PP (calcination temperatures : 650 – 740°C) and SG (calcination temperatures : 450 – 600°C), based on wet-chemical syntheses were used in the present study.^{1,2} The chemical composition of both series of a-YAB powders is stoichiometrically close to crystalline $YAl_3(BO_3)_4$ (c-YAB). The powders are labeled as PP-x and SG-x, where x represents the final heat-treatment (calcination) temperature in oxidizing atmosphere in degrees Celsius. The powders exhibit a clear white to pale yellow colored tint with the increase in calcination temperature in both series. The $Y_3Al_5O_{12}:Ce^{3+}$ (YAG:Ce),

ZnGa₂O₄:Cr³⁺ (ZGO:Cr) polycrystalline phosphors and Ce³⁺: borate glass were also used for comparison. The detailed synthesis procedure for the studied samples is described in the supporting information (SI) and in literature [1,2,23]. The phase purity of polycrystalline YAG:Ce and ZGO:Cr, as well as the amorphous nature of a-YAB powder was confirmed using X-ray diffraction analysis (supporting information, Figure S1)

The PL spectra of the powders were obtained under 254 nm excitation and the emission signals were recorded using a calibrated CCD detector (Acton Pixis 100, Princeton Instruments). A similar setup was used for X-ray radioluminescence (RL), where 1.54 Å Cu K_α X-ray was used as excitation. For CL spectroscopy, a Hitachi S3400-N scanning electron microscope was used, combined with a fiber-coupled spectrometer (Acton SP2300 monochromator and ProEM 1600 EMCCD camera, Princeton Instruments). The electron microstructure was studied using backscattered electrons. Energy dispersive X-ray imaging of the Y L_α (1.922 keV), Al K_α (1.486 keV) and O K_α (0.525 keV) lines was used for the elemental analysis at the microscopic level. The SEM was operated at 20kV potential and 50 μA current density under 25 Pa pressure to avoid charging of the samples. The samples were prepared by spreading fine powder particles on a carbon tape attached to the sample mount.

Results and Discussion

Figure 2 presents the SEM images of the microstructure and the related CL emission of SG-600 a-YAB powder. All particles exhibit CL emission and the particles' morphology could clearly be reproduced in the CL mapping. The PP series powders also exhibit homogeneous CL emission [24]. It has been observed that the CL signals are weak in a-YAB powders compared to the traditional inorganic phosphor materials. On comparing the CL response with respect to the traditional crystalline phosphors, such as ZnGa₂O₄: Cr³⁺ (ZGO:Cr), the CL emission intensity in a-YAB powders is several orders of magnitude lower (Figure 3a). The intensity is even weaker for the a-YAB powders synthesized at lower calcination temperatures (Supporting Information, Figure S2).

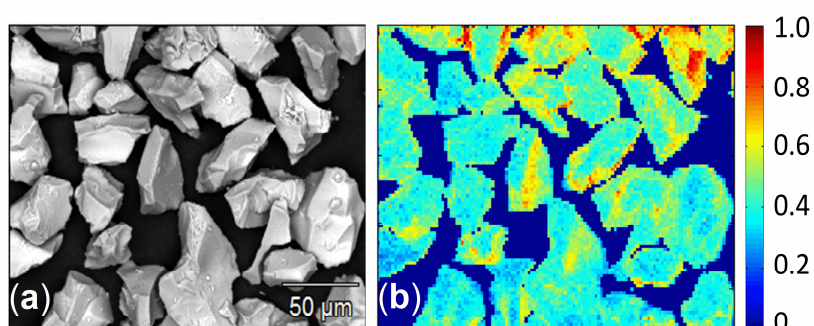


Figure 2: SEM microstructure (a) and corresponding CL intensity map (b) of SG-600 powder.

The low intensity for CL signals in a-YAB powders may be due to the amorphous nature of the a-YAB host. Amorphous or glassy hosts are usually less efficient in trapping ionizing radiations and delivering the excitation energy to the luminescent active centers [23]. The

presence of several defects, including the dangling bonds, various point defects, etc., are inherent to the amorphous structure that can easily facilitate a swift non-radiative recombination of the excitonic e-h (electron-hole) pairs created by high energy irradiation. Moreover, the organic luminophores exhibit poor response to high energy ionizing excitations, and even undergo degradation under continuous exposure (Supporting Information, Figure S3), though the respective PL signals are stable with respect to the excitation duration and temperature (Supporting Information, Figures S4, S5). Similarly to the CL, the X-ray radioluminescence (RL) intensity is weak in a-YAB powders compared to the traditional lanthanide doped luminescent materials. Figure 3b presents the RL response of PP-740 a-YAB powder compared with the polycrystalline YAG:Ce phosphor and Ce-doped borate glass. It is interesting to see that the YAG:Ce exhibits almost seven orders of magnitude more intense RL over a-YAB, whereas two orders of enhancement is observed in Ce³⁺ doped glass. The intensity difference also reflects the polycrystalline and glassy nature of the respective host materials, i.e. YAG and borate glass, respectively.

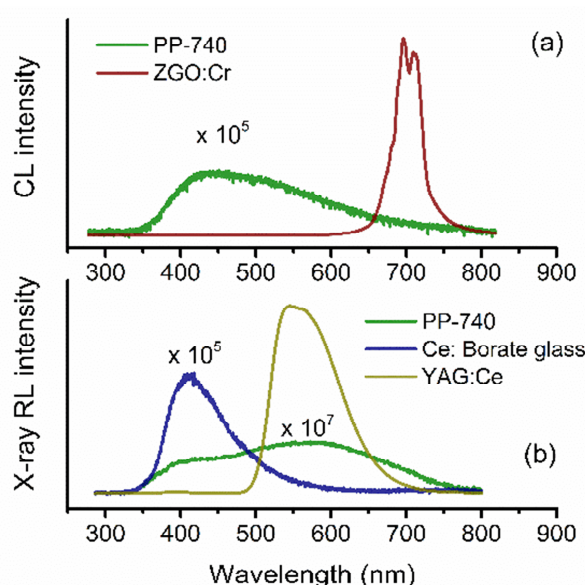


Figure 3: CL spectra (a) and X-ray RL spectra (b) comparison between PP-740 a-YAB powder and representative traditional luminescent materials.

From Figure 3, it can be noticed that the CL spectral profile of PP-740 a-YAB powder exhibits good resemblance with its PL spectral profile (PP-740 powder in Figure 1), whereas the RL profile is significantly different. The dominant blue region emission in the PL has slightly reduced in CL, but it is significantly reduced in the RL spectrum. This is consistent with the fact that the a-YAB powder exhibits several emitting centers with varied energy levels and the relatively deeper penetration depth of the used X-ray radiation (several tens of μm) might induce radiation trapping of higher energy (violet-blue region) emissions in the RL emission signals [15,24]. The penetration depth in CL is expected to be of the order of 3-4 μm at the used electron energy in a-YAB host, so the reabsorption is relatively weaker (Supporting Information, Figure S6).

The multiple emissions in a-YAB powder arise from different emitting centers, whose relative abundance is controlled by the calcination temperature [15]. This causes the

broadening of predominantly intense violet-blue region emission as the calcination temperature increases. Simultaneously, the longer wavelength emissions become more distinctive at the expense of violet-blue emissions. Although this variation in the relative prominence of different emitting centers could be observed experimentally, the origin of this systematic bathochromic shift in emission is yet to be understood. As discussed earlier, it can either be due to the transformation of emitting centers, such as the π -conjugation of PAH compounds or due to the changes in functional groups, or can also be due to the changes in the chemical environment of the surrounding host matrix. An enlarged π -conjugation reduces the energy of electronic transitions in PAH compounds. Similarly, the changes in functional group or the chemical polarization of surrounding host matrix can modify the energy levels of the emitting centers. The microscopic analysis, such as the powder microstructure and cathodoluminescence could be interesting in this regard to understand the evolution of the a-YAB matrix with temperature and find any relation with luminescence broadening.

Figure 4 presents the SEM microstructure images of the PP and SG series powders calcined at various temperatures. For the entire PP series, the images do not exhibit noticeable contrast difference amongst particles suggesting a near homogeneous elemental distribution (Supporting Information, Figure S7) [25]. However, the SG series powders show interesting microstructural evolution as the synthesis temperature increases. For powders prepared at low temperature, the microstructure reveals particles with dark and bright regions. As the dark/bright color difference in SEM imaging based on backscattered electrons mainly originates from the difference in average atomic weights of constituent elements [26], this suggests an elemental inhomogeneity. The darker particles, which have a relatively lower average weight, slowly vanish as the calcination temperature increases. For a calcination temperature of 570°C, nearly homogeneously bright particles are obtained with the SG synthesis. Figure 5 presents the CL emission spectra of some PP and SG powders. Similar to PL, the CL emission also exhibits spectral broadening and a redshift in the peak position with increasing calcination temperature.

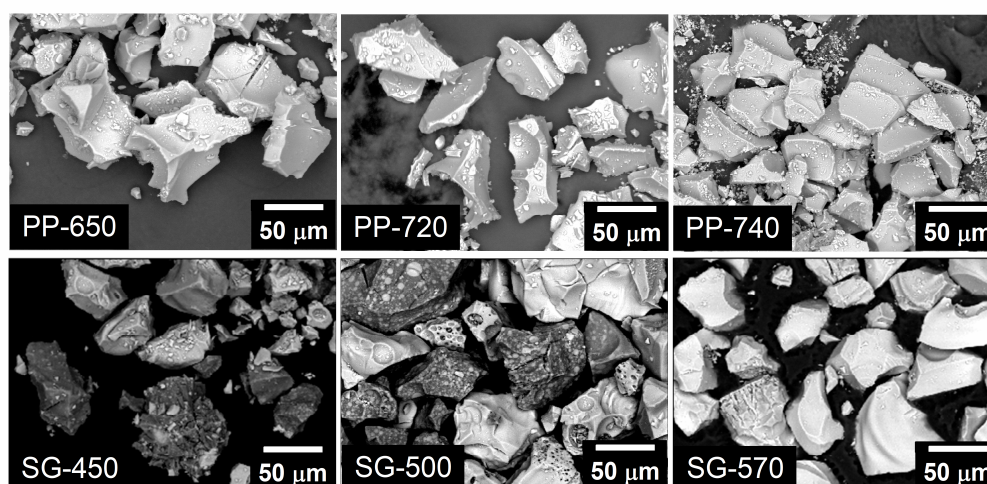


Figure 4: Influence of calcination temperature on the microstructure of a-YAB powder in the PP (top) and SG series (bottom), when imaged in the electron backscattered imaging SEM mode.

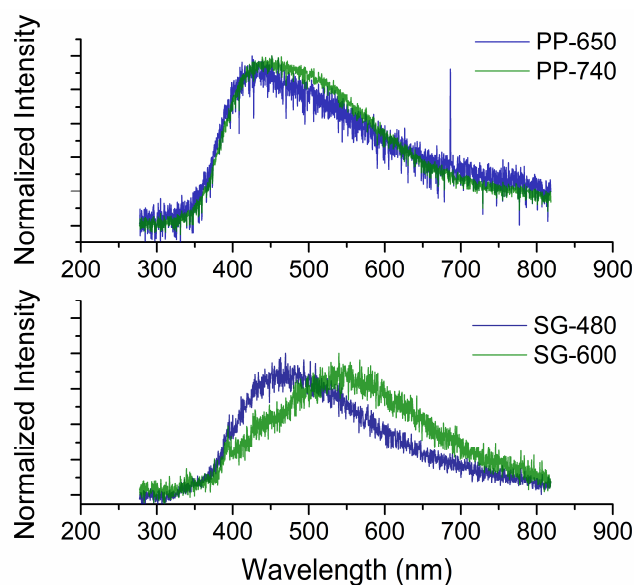


Figure 5: CL emission spectra of PP-series and SG-series a-YAB powders.

Figure 6(a) presents the EDX elemental analysis of particles in the SG-480 powder. It suggests that the dark region particles are exclusively yttrium deficient, whereas aluminum seems well distributed in all the particles. These observations suggest that the dark regions are enriched in boron, associated with aluminum, however boron, due to its low atomic weight, could not directly be detected by EDX. It is worth noting here that despite the presence of such chemical differences, the CL emission profile does not exhibit significant deviation among different particles and peaks at nearly same positions in all the particles of respective samples (Supporting Information, Figures S8, S9). Nevertheless, a more reliable comparative analysis of CL emission profile of different particles is limited due to the different levels of signal to noise ratio, varied penetration depths, exposure based degradation and overall weak CL signals. Interestingly, at 570°C and higher calcination temperatures, particles do not exhibit such distinct elemental inhomogeneity (Figure 4 and Supporting Information, Figure S7). The gradual disappearance of dark regions in particles is accompanied with a systematic appearance of bright spots, whose abundance and dimensions grows for higher calcination temperature. Figure 6(b) shows the elemental mapping of such a particle exhibiting bright region spots representing yttrium rich regions. This points at an increase of diffusion dynamics of atom species within the particles when the calcination temperature increase. Accordingly, the yttrium rich regions appear on the surface of the dark particles, and start to grow bigger with the increase in calcination temperature (Figure 7a, b). Eventually, the bright spots start to coalesce and lead to completely bright particles with near homogeneous elemental distribution (Figure 7c-e).

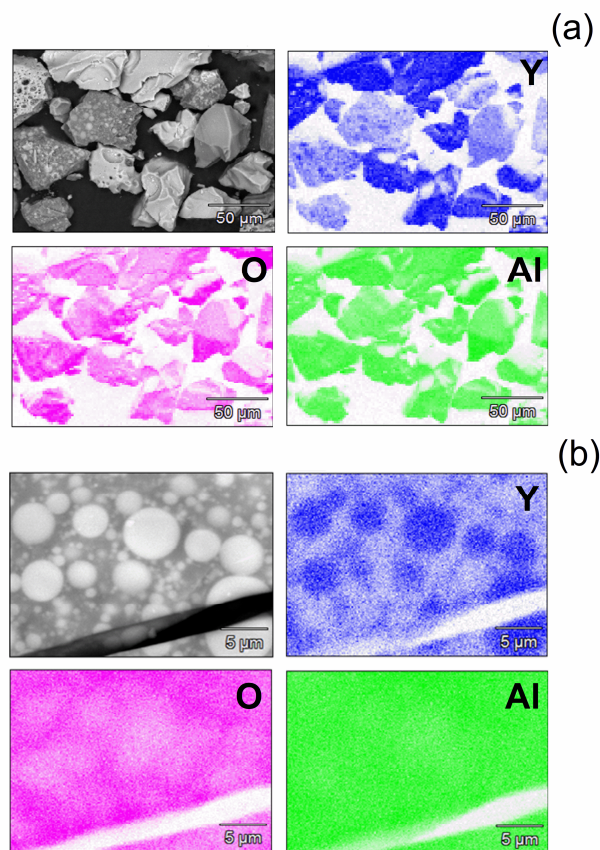


Figure 6: (a) SEM microstructure and EDX elemental mapping of the elements Al, Y and O in SG-480 powder. (b) The enlarged view of a particle possessing both dark and bright regions. A more saturated color represents a higher density of the elements.

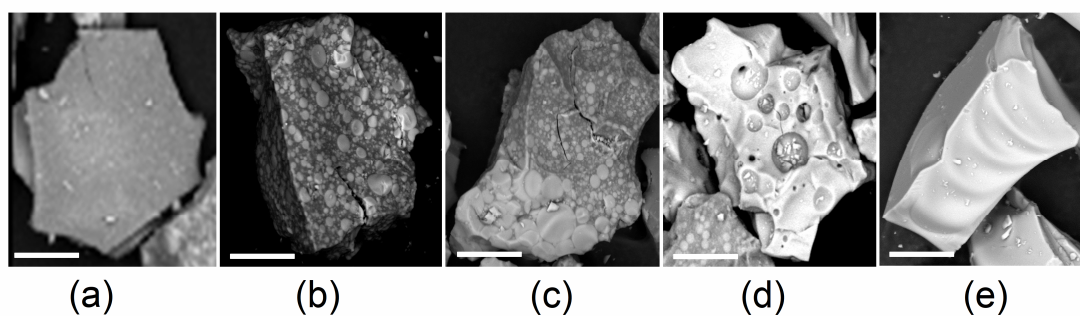


Figure 7: SEM microstructure of a-YAB powder particles exhibiting different stages (a-e). (a) is from SG-450 powder, (e) is from SG-570 powder and (b-d) are from intermediate temperature calcined powders. Scale bars represent 25 μm .

To get further insight on the diffusion reaction, the particles were crushed to see the cross-sectional EDX elemental distribution. Figure 8 shows the microstructure as observed in SEM and EDX mapping of darker particles after gently crushing them. It is clear that mainly the surface layer of the dark region particles is deficient in yttrium. The low density aluminum-borate matrix forms the surface region, whereas the dense yttrium-aluminate matrix is segregated in the core region. With increase in calcination temperature, the elements diffuse

more effectively leading to the homogeneous yttrium-aluminum-borate matrix. It is evident that the presence of darker particles gradually decreases from SG-450 to SG-570, where the SG-570 does not contain any difference between or within particles. The chemical composition (Al:Y) for SG-570, SG-600 and all the PP-x series powders is similar to c-YAB suggesting a nearly homogeneous microscopic elemental distribution in these powders. Indeed, above 570°C nearly homogeneous particles are obtained with a Y:Al ratio about 1.1 close to that of the crystalline YAB composition (Supporting Information, Figure S10).

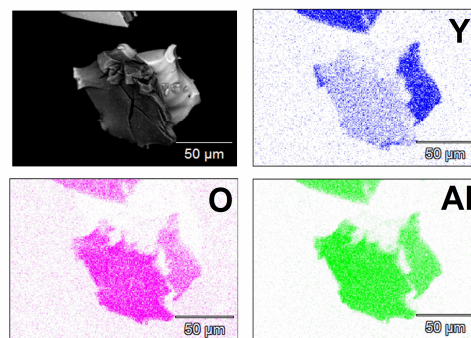


Figure 8: Microstructure (SEM image, top left) and EDX elemental maps of the elements Y, Al and O in a crushed dark particle. A more saturated color represents a higher density of the elements.

Consequently, the SG-x series powders show significant structural variations, whereas the PP-x series powders are essentially homogeneous. For both series of powders, the PL and CL emission spectra exhibit spectral broadening as a function of calcination temperature. As the calcination temperature primarily controls the elemental diffusion, an interesting microstructural evolution in SG series a-YAB powders could be observed. But any direct relation between powder microscopic properties and the PL band broadening could not be established. It is therefore evident that the luminescence broadening as a function of calcination process is more intrinsic to the luminescent centers rather than the microscopic level chemical properties of a-YAB powders. It might be controlled by immediate changes in and around the luminescent centers brought about due to thermal treatment during calcination process. The chemical surrounding at immediate neighborhood of emitting PAH compounds can be decisive in this respect, which may be limited to a few atomic layers and therefore could not be resolved in present investigation. Moreover, the other effects such as pi-conjugation enlargement and the effect of functional groups could also be responsible for the bathochromic shift and needs further investigation.

Conclusions

In summary, the a-YAB powders exhibit weak but homogeneous cathodoluminescence emission. The microstructural analysis revealed that the sol-gel synthesized a-YAB powders exhibit elemental inhomogeneity at low calcination temperature (<570°C) and systematically attain a homogeneous a-YAB matrix composition with increase in calcination temperature. This inhomogeneity could not be observed in polymeric precursor synthesized powders. Despite

these structural differences, the PL and CL spectra for both syntheses showed a similar spectral broadening with increasing calcination temperature within the respective optimum temperature range. These results suggest that the microscopic level elemental homogeneity and its diffusion dynamics do not exhibit significant influence on the spectral broadening of the luminescence in α -YAB powders during the calcination process, but that this might be controlled by more intrinsic effects in and around the luminescent centers.

Acknowledgements:

This work was supported by the ANR LuminoPhorLED (ANR-14-CE05-0033) and Lumicor SBO130030 project grants. Authors would like to thank Prof. Isabelle Gautier-Luneau and Dr. Alain Ibanez, CNRS-Inst. NEEL, Grenoble for providing the samples and fruitful suggestions.

References

1. A. D Sontakke, A. Ferrier, P. Burner, V. F Guimarães, M. Salaün, V. Maurel, I. Gautier-Luneau, A. Ibanez, B. Viana, Afterglow luminescence in wet-chemically synthesized inorganic materials : ultra-long room temperature phosphorescence instead of persistent luminescence, *J. Phys. Chem. Lett.* 8 (2017) 4735-4739.
2. P. Burner, A. D Sontakke, M. Salaün, M. Bardet, J. M. Mouesca, S. Gambarelli, A. L. Barra, A. Ferrier, B. Viana, A. Ibanez, V. Maurel, I. Gautier-Luneau, Evidence of organic luminescent centers in sol-gel-synthesized yttrium aluminum borate matrix leading to bright visible emission, *Angew. Chem. Int. Ed.* 56 (2017) 13995-13998.
3. V. F. Guimaraes, L. J. Q. Maia, I. Gautier-Luneau, C. Bouchard, A. C. Hernandez, F. Thomas, A. Ferrier, B. Viana, A. Ibanez, Towards a new generation of white phosphors for solid state lighting using glassy yttrium aluminoborates, *J. Mater. Chem. C* 3 (2015) 5795-5802.
4. S. K. Soon, H. F. Wang, X. P. Yan, Engineering persistent luminescence nanoparticles for biological applications: from biosensing/bioimaging to theranostics, *Acc. Chem. Res.* 51 (2018) 1131-1143.
5. A. Feng, P. F. Smet, A review of mechanoluminescence in inorganic solids: compounds, mechanisms, models and applications, *Materials*, 11 (2018) 484 (1-56).
6. Y. H. Kim, N. S. M. Viswanath, S. Unithrattil, H. J. Kim, W. B. Im, Review—phosphor plates for high-power LED applications: challenges and opportunities toward perfect lighting, *ECS J. Sol. State Sci. Technol.* 7 (2018) R3134-R3147.
7. P. F. Smet, A. B. Parmentier, D. Poelman, Selecting conversion phosphors for white light-emitting diodes, *J. Electrochem. Soc.* 158 (2011) R37-R54.
8. D. Dutczak, T. Jüstel, C. Ronda, A. Meijerink, Eu^{2+} luminescence in strontium aluminates, *Phys. Chem. Chem. Phys.* 17 (2015) 15236-15249.
9. N. C. George, A. J. Pell, G. Dantelle, K. Page, A. Llobet, M. Balasubramanian, G. Pintacuda, B. F. Chmelka, R. Seshadri, Local environments of dilute activator ions in the solid-state lighting phosphor $\text{Y}_{3-x}\text{Ce}_x\text{Al}_5\text{O}_{12}$, *Chem. Mater.* 25 (2013) 3979-3995.

10. J. J. H. A. van Hest, G. A. Blab, H. C. Gerritsen, C. de Mello Donega, A. Meijerink, Probing the Influence of disorder on lanthanide luminescence using Eu-doped LaPO₄ nanoparticles, *J. Phys. Chem. C* 121 (2017) 19373-19382.
11. S. M. Borisov, K. Gatterer, B. Bitschnau, I. Klimant, Preparation and characterization of chromium(III)-activated yttrium aluminum borate: a new thermographic phosphor for optical sensing and imaging at ambient temperatures, *J. Phys. Chem. C*, 114 (2010) 9118-9124.
12. H. F. Sijbom, R. Verstraete, J. J. Joos, D. Poelman, P. F. Smet, K₂SiF₆:Mn⁴⁺ as a red phosphor for displays and warm-white LEDs: A review of properties and perspectives, *Opt. Mater. Exp.* 7 (2017) 3332-3365.
13. J. Patarin, Mild methods for removing organic templates from inorganic host materials, *Angew. Chem. Int. Ed.* 43 (2004) 3878-3880.
14. S. H. Hong, W. J. Shim, L. Hong, Methods of analysing chemicals associated with microplastics: A review, *Anal. Methods* 9 (2017) 1361-1368.
15. A. D. Sontakke, J.-M. Mouesca, V. Castaing, A. Ferrier, M. Salaün, I. Gautier-Luneau, V. Maurel, A. Ibanez, B. Viana, Time-gated triplet-state optical spectroscopy to decipher organic luminophores embedded in rigid matrices, *Phys. Chem. Chem. Phys.* 20 (2018)23294-23300.
16. H. Meier, J. Gerold, H. Kolshorn, B. Muhling, Extension of conjugation leading to bathochromic or hypsochromic effects in OPV series, *Chem. Eur. J.* 10 (2004) 360-370.
17. A. Kuchařová, J. Götze, Š. Šachlová, Z. Pertold, R. Přikryl, Microscopy and cathodoluminescence spectroscopy characterization of quartz exhibiting different alkali-silica reaction potential, *Microsc. Microanal.* 22 (2016) 189-198.
18. B. Dierre, X. L. Yuan, K. Inoue, N. Hirosaki, R.-J. Xie, T. Sekiguchi, Role of Si in the luminescence of AlN:Eu,Si phosphors, *J. Am. Ceram. Soc.* 92 (2009) 1272-1275.
19. L. I. D. J. Martin, D. Poelman, P. F. Smet, J. J. Joos, Microscopic study of dopant distribution in europium doped SrGa₂S₄: Impact on thermal quenching and phosphor performance, *ECS J. Sol. State Sci. Technol.* 7 (2018) R3052-R3056.
20. S. Abe, J. J. Joos, L. I. D. J. Martin, Z. Hens, and P. F. Smet, Hybrid remote quantum dot/powder phosphor designs for display backlights, *Light Sci. Appl.*, 6 (2017) e16271 (1-9).
21. J. J. Joos, K. Korthout, S. Nikitenko, D. Poelman, and P. F. Smet, Origin of saturated green emission from europium in zinc thiogallate, *Opt. Mater. Express*, 3 (2013) 1338-1350.
22. M. Broxtermann, D. Den Engelsen, G.R. Fern, P. Harris, T.G. Ireland, T. Jüstel, J. Silver, Cathodoluminescence and photoluminescence of YPO₄: Pr³⁺, Y₂SiO₅: Pr³⁺, YBO₃: Pr³⁺ and YPO₄: Bi³⁺, *ECS J. Solid State Sci. Technol.*, 6 (2017) R47-R52.
23. A. D. Sontakke, J. Ueda, J. Xu, K. Asami, M. Katayama, Y. Inada, S. Tanabe, A comparison on Ce³⁺ luminescence in borate glass and YAG ceramic: Understanding the role of host's characteristic, *J. Phys. Chem. C* 120 (2016) 17683-17691.
24. V. F. Guimaraes, M. Salaün, P. Burner, L. J. Q. Maia, A. Ferrier, B. Viana, I. Gautier-Luneau, A. Ibanez, Controlled preparation of aluminum borate powders for the development of defect-related phosphors for warm white LED lighting, *Sol. State Sci.* 65 (2017) 6-14.
25. M. Berz, K. Makino, W. Wan, *An Introduction to Beam Physics*, CRC press, 2014.
26. G. E. Lloyd, Atomic number and crystallographic contrast images with the SEM: A review of backscattered electron techniques, *Mineral. Mag.* 51 (1987) 3-19.